1996

Data Compression Based on the Cubic B-Spline Wavelet With Uniform Two-Scale Relation

S. K. Yang
Old Dominion University

C. H. Cooke
Old Dominion University

Original Publication Citation

Yang, S. K., & Cooke, C. H. (1996). Data compression based on the cubic B-spline wavelet with uniform two-scale relation. *Mathematical and Computer Modelling*, *23*(7), 73-88. doi:10.1016/0895-7177(96)00030-1

Pergamon

Mathl. Comput. Modelling Vol. 23, No. 7, pp. 73–88, 1996

0895-7177/96 $15.00 + 0.00

S0895-7177(96)00030-1

Data Compression Based on the Cubic B-Spline Wavelet with Uniform Two-Scale Relation

S. K. YANG AND C. H. COOKE
Department of Mathematics and Statistics
Old Dominion University, Norfolk, VA 23529, U.S.A.

(Received July 1995; accepted August 1995)

Abstract—The aim of this paper is to investigate the potential artificial compression which can be achieved using an interval multiresolution analysis based on a semiorthogonal cubic B-spline wavelet. The Chui-Quak [1] spline multiresolution analysis for the finite interval has been modified [2] so as to be characterized by natural spline projection and uniform two-scale relation. Strengths and weaknesses of the semiorthogonal wavelet as regards artificial compression and data smoothing by the method of thresholding wavelet coefficients are indicated.

Keywords—Semiorthogonal B-spline wavelet, Data compression, Boundary wavelets, Thresholding.

1. INTRODUCTION

Classical approaches to wavelet construction deal with multiresolution analysis (MRA) on the entire real axis [3,4]. More recently, the construction of suitable wavelets for bounded intervals has become of interest [1,5,6], primarily as a means for elimination of edge effects in image analysis. Such constructions are usually directed toward synthesis of orthogonal or semiorthogonal wavelets. The two classes have an underlying common structure, yet exhibit diversity in methodology and complexity of an associated computational algorithm.

Meyer [7] has adapted the orthogonal wavelets of Daubechies [4] to the bounded interval. However, his procedure for obtaining orthogonality of boundary scaling functions encounters an ill-conditioned matrix and ensuing numerical instability as matrix size increases. This mishap motivated Cohen, Daubechies, and Vial [5] to take an approach, whereby boundary scaling functions are no longer obtained by restriction to the interval of the customary scaling functions. This causes some inconvenience in reconstruction, as various two scale relations are required near boundaries.

Perhaps anticipating numerical instabilities if proceeding otherwise, Chui-Quak [1] construct (and Quak-Weyrich [6] implement) semiorthogonal spline wavelets for the interval, introducing special boundary scaling functions which possess multiple nodes at an endpoint. Intuitively, it appears unnatural to harbor the inconvenience of scaling functions possessing two scale relations which vary over the interval. There is little reason to suspect that otherwise numerical instabilities might occur, as for spline wavelets orthogonalization is not a factor.

Consequently, in a companion paper [2] there has been reexamined, for the case of cubic B-spline wavelets with compact support, the feasibility of employing an alternative MRA for the interval. The modification is as follows. First, boundary scaling functions which are the restriction to the interval of cubic B-spline translates are retained. The reconstruction process is now simplified,

as a two-scale equation which is the interval restriction of the classical two-scale relation applies uniformly. Moreover, by employing nested spaces of natural cubic splines for the MRA, it is seen that distortion of images is diminished. The revised boundary wavelets do not markedly differ in appearance from those of Chui-Quak [1,6]. As numerical results appear equivalent to those of [6], whereas operation count is improved and numerical instability is not experienced, the effort is deemed successful.

A natural question from the wavelet user community concerns the plethora of wavelets on the market (orthogonal, semiorthogonal, biorthogonal, etc.); namely, what are their relative strengths and weaknesses? This question will be explored here, in terms of the determining potential merits of semiorthogonal spline wavelets, as regards data compression and data smoothing, employing the usual devices in thresholding wavelet coefficients. We find nothing to become excited about as regards data smoothing. However, more success is achieved in the area of data compression, as without the tree searches of best basis schemes, compression ratios of up to 40-to-1 are obtained, where the usual error tolerance of no more than 5% relative error is the standard.

As the research presented here depends strongly upon the previous work, for clarity of foundations it will be necessary to review the boundary wavelet machinery previously developed [2].

2. PRELIMINARY CONSIDERATIONS

Quak and Weyrich [6] review the axioms of Mallat [8] required of MRA for $L_2(R)$, and stipulate the requirements for MRA adapted to an interval. For MRA on $L_2[a,b]$, the sequence of function subspaces can be infinite only in the direction corresponding to mesh refinement. There is some initial space V_1 with sufficient nodes to contain entirely the support of at least one inner wavelet, and a sequence of nested spaces

$$\cdots V_{-2} \subset V_{-1} \subset V_0 \subset V_1 \subset \cdots \subset V_J \subset \cdots . \tag{1}$$

The spaces V_J are related by

$$V_{J+1} = V_J \oplus W_J, \tag{2}$$

where W_J is the orthogonal complement in V_{J+1} of V_J. The most fundamental requirement of an MRA is that there is a scaling function $\phi(x)$ such that, for finitely many k, the scaling function translations satisfy

$$\phi(x) \in V_0 \Leftrightarrow \phi\left(2^J x - k\right) \in V_J, \tag{3}$$

and the linear span of these translations covers V_J.

In the sequel, attention is directed to the interval $[0,8]$. V_0 is the space of natural cubic splines with (at most) simple nodes at $0,1,2,3,4,5,6,7,8$. Thus, V_J is the space of natural cubic splines with nodes at $k/2^J$, $k = 0,1,\ldots,2^{J+3}$.

Generally, scaling functions inhabit an approximation space, while wavelets are members of the orthogonal complement. If $\phi(x) \in V_0$ is a scaling function, a finite number of translations, $\phi(2^J x - k)$, together with an appropriate number of boundary scaling functions, constitute a basis for V_J. In this research, a boundary scaling function is simply the interval restriction of some translation of the interior scaling function.

When the V_J are spaces of natural cubic splines, one can choose as interior scaling function for V_0 the cardinal B-spline (see [9]) $N(x) = 4[0,1,2,3,4]_t(t-x)^3{}_+$. Here, $[.,\ldots,.]_t$ is the 4^{th} divided difference of $(t-x)^3{}_+$. The corresponding two scale relation is

$$N(x) = \sum_{k=-2}^{2} p_k N(2x - k - 2), \tag{4}$$

where p_k is an element of [3]

$$P_c = \frac{1}{8}[1,4,6,4,1]. \tag{5}$$

On the interval, $\psi(x) \in W_0$ is an *inner wavelet* if it possesses no support at the endpoints, and some finite collection $\psi(2^J x - k)$, together with any required boundary wavelets $\psi_l^B(2^J x)$ constitute a basis for W_J. The inner wavelet used in the sequel is the compactly supported Chui-Wang cubic B-wavelet [3]. For each space W_J, $J \geq 0$, three boundary wavelets are required at each end of the interval, together with $2^{J+3} - 6$ inner wavelet translations. Translations of a boundary wavelet are of no interest.

3. MAPLE DERIVATION OF BOUNDARY WAVELETS

Boundary wavelets are derived initially for the space W_0. For $J = 1, 2, \ldots, N$, a W_J wavelet is a (possibly translated) scaled version of some W_0 wavelet. Wavelets for the ultra-coarse spaces W_J, $J = -1, -2, -3$ all have support on at least one boundary: no inner wavelet exists. Thus, a unique wavelet derivation is required for each space. In the literature these spaces usually have been neglected [1,6].

The space W_0 allows two inner wavelets, whose supports are [0,7] and [1,8]. Wavelets for this space are designated as

$$\psi_{2j-1}(x), \qquad j = 1, \ldots, 8 \tag{6}$$

according to the indices of the nodes which disappear when a V_1 function is projected on V_0, where the indices $j = 4, 5$ correspond to inner wavelets. Subsequently, scaled versions of these wavelets which are in V_J will be referred to as

$$\psi_k^J(x), \qquad k = 1, 3, \ldots, N-1 \tag{7}$$

where $N = 2^{J+3}$, and the first three and last three index values refer to boundary wavelets.

The necessity for a boundary wavelet arises when it is observed that left (right) translations of ψ_4 (ψ_5) are no longer orthogonal to V_0. Indeed, the only requirement for constructing boundary wavelets in W_0 is that

(a) they are orthogonal to V_0, and
(b) the collection (5) is linearly independent and spans W_0.

Linear independence can be arranged as follows [1]. Let $\Psi_k = \psi_{2k+1}(x)$ and choose the left boundary wavelets Ψ_0, Ψ_1, Ψ_2 to have support [0,4], [0,5], [0,6], whereas the right boundary wavelets Ψ_5, Ψ_6, and Ψ_7 satisfy $\Psi_{7-l}(x) = \Psi_l(8 - x)$, $l = 0, 1, 2$.

To satisfy condition (a), the constants C_k^j in the equations

$$\Psi_j(x) = \sum_{k=-3}^{2j+4} C_k^j N(2x - k), \qquad j = 0, 1, 2 \tag{8}$$

are chosen such that Ψ_j is orthogonal to every function $N(x - i)$ with which it shares support. For fixed j, this leads to solving a homogeneous system of $7 + j$ equations in $8 + 2j$ unknowns.

Latitude in solving these systems is removed by the principle of minimal interference with interior interaction; the innermost profile of a boundary wavelet is chosen insofar as possible to conform to the corresponding profile of the Chui-Wang [1,3] inner wavelet. This choice is made possible because $j + 1$ of the associated determining equations for boundary wavelet Ψ_j will be identical to those required for the inner wavelet. By substituting inner wavelet coefficients, for each j this reduces to finding the unique solution of a system involving six inhomogeneous equations in six unknowns. Set up and solution is accomplished using the Maple symbolic algebraic manipulation package. Coefficients of the boundary and inner wavelets are given in Table 1. Figures 1–4 show wavelet profiles. As may be seen, there is no marked difference in appearance between the present boundary wavelets and those of Chui-Quak [1,6].

Table 1. Natural spline wavelets.

Coefficients Of The Two-Scale Relations For Cubic Wavelets				
i	First Boundary Wavelet	Second Boundary Wavelet	Third Boundary Wavelet	Inner Wavelet
−3	$\frac{-451866263}{28100016}$	$\frac{657311485}{196700112}$	$\frac{-419725}{24587514}$	0
−2	$\frac{157179839}{56200032}$	$\frac{-138630091}{393400224}$	$\frac{348403}{196700112}$	0
−1	$\frac{-4718657}{4014288}$	$\frac{-21954047}{196700112}$	$\frac{-168239}{49175028}$	0
0	$\frac{633094403}{1124000640}$	$\frac{7917027}{17841280}$	$\frac{743093}{17841280}$	$\frac{1}{40320}$
1	$\frac{-19083341}{93666720}$	$\frac{-1181603407}{1967001120}$	$\frac{-385603003}{1967001120}$	$\frac{-31}{10080}$
2	$\frac{668851}{16057152}$	$\frac{1202163647}{2622668160}$	$\frac{3606559267}{7868004480}$	$\frac{559}{13440}$
3	$\frac{-31}{10080}$	$\frac{-247}{1260}$	$\frac{-337}{560}$	$\frac{-247}{1260}$
4	$\frac{1}{40320}$	$\frac{559}{13440}$	$\frac{9241}{20160}$	$\frac{9241}{20160}$
5	0	$\frac{-31}{10080}$	$\frac{-247}{1260}$	$\frac{-337}{560}$
6	0	$\frac{1}{40320}$	$\frac{559}{13440}$	$\frac{9241}{20160}$
7	0	0	$\frac{-31}{10080}$	$\frac{-247}{1260}$
8	0	0	$\frac{1}{40320}$	$\frac{559}{13440}$
9	0	0	0	$\frac{-31}{10080}$
10	0	0	0	$\frac{1}{40320}$

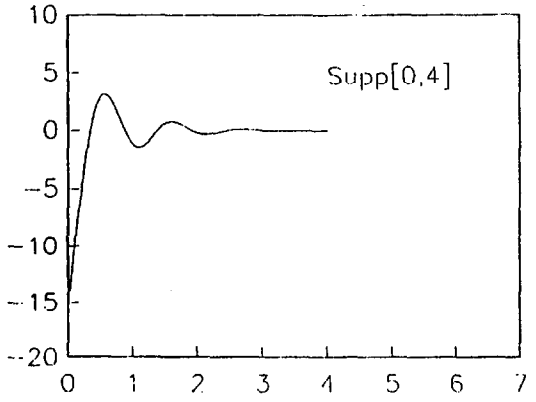

Figure 1. First boundary wavelet.

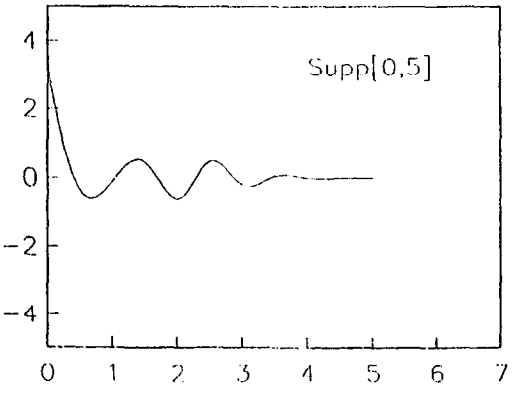

Figure 2. Second boundary wavelet.

4. FRONTAL DECOMPOSITION

Let V_J be the space of natural cubic splines with the most simple nodes at x_k, $k = 0, 1, \ldots, N$. Here, $N = 2^{J+3}$, h is the node spacing, and let $\phi_k^J(x) = N(2^J x - k + 4)$, $k = -1, \ldots, N+1$ be the cardinal B-spline basis for V_J.

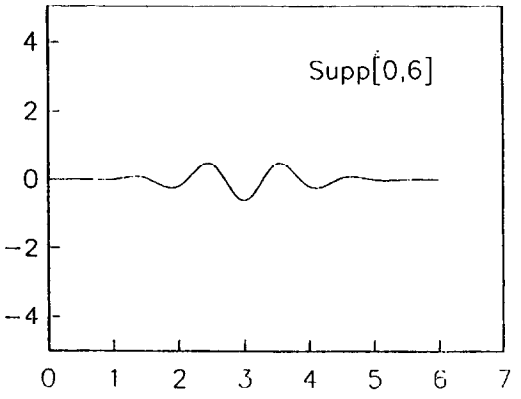

Figure 3. Third boundary wavelet.

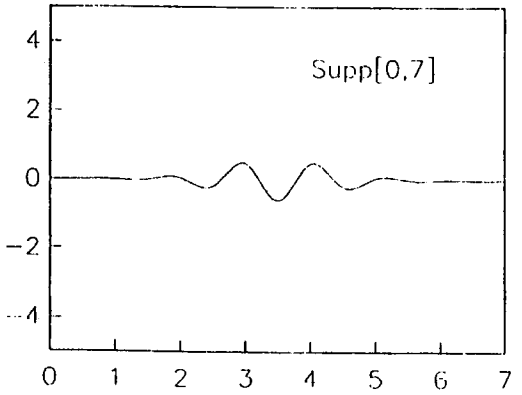

Figure 4. Inner wavelet.

If y_j, $j = 0, 1, \ldots, N$ are sampled data values from some function $f(x)$, then

$$P_h f = \sum_{k=-1}^{N+1} C_k \phi_k^J(x), \tag{9}$$

is a projection on V_J, provided the following requirements are satisfied:

$$C_0 = y_0 \qquad C_N = y_N, \tag{10}$$

$$C_{i-1} + 4C_i + C_{i+1} = 6y_i, \qquad i = 1, 2, \ldots, N-1, \tag{11}$$

together with the conditions for a natural spline fit

$$C_{-1} = 2C_0 - C_1 \qquad C_{N+1} = 2C_N - C_{N-1}. \tag{12}$$

The most desirable feature of a multiresolution analysis is provision of means to calculate the relation between the projection $P_h f$ on the fine grid V_j and its best natural spline approximation $P_{2h} f$ in the coarser space V_{J-1}:

$$P_h f = P_{2h} f + W_h(x), \tag{13}$$

where

$$P_{2h} f = \sum_{k=-1}^{N/2+1} c_{2k} \phi_k^{J-1}(x). \tag{14}$$

Here, even indices are used to emphasize the disappearance of odd-indexed nodes under projection, and the natural spline conditions are

$$c_{-2} = 2c_0 - c_2 \qquad c_{N+2} = 2c_N - c_{N-2}. \tag{15}$$

In particular, the function $W_h(x)$ is to be expressed in terms of a scaled version applicable to W_{J-1} of the B-wavelet basis for W_0 derived in the previous section:

$$W_h(x) = \sum_{k=1}^{N/2} d_k \Psi_{2k-1}^J(x), \tag{16}$$

where the indexing associates a wavelet translation with each odd-indexed node on the fine mesh. Boundary wavelets are encountered for the first three and last three index values.

Iteration of the projection (20,21) over successively coarser grids is referred to as *decomposition* of the function $f(x)$ into its wavelet components. There results

$$P_h f = P_{2^j h} f + \sum_{k=0}^{j-1} W_{2^k h}(x). \tag{17}$$

The reverse process of building up the function from knowledge of the c_k, d_k at each level is referred to as *reconstruction*.

For B-wavelets in $L_2(R)$, decomposition using pyramid schemes usually leads to concomitant development of a boundary layer of error near interval endpoints, caused by truncation of weight sequences [3]. The point of developing MRA for the finite interval is to avoid this difficulty. A frontal decomposition scheme for which edge effects have been eliminated is now presented. Reconstruction proceeds as usual by a reverse pyramid scheme [3], suitably modified to account for boundaries and presence of boundary wavelets.

By the theory of approximation in Hilbert space, the best approximant in V_{J-1} to a given natural spline $P_h f$ is the unique solution of the following constrained optimization problem:

$$\text{Min} \int_{x_0}^{x_N} \{P_h f - P_{2h} f\}^2 \, dx. \tag{18}$$

The solution for the even indexed variables c_{2k}, $k = 0, 1, \ldots, M = N/2$ is obtained from solving the banded system

$$AC = F, \tag{19}$$

where

$$A = \begin{bmatrix}
\frac{451}{630} & \frac{1013}{2520} & \frac{61}{1260} & \frac{1}{2520} & 0 & 0 & 0 & 0 & 0 \\
\frac{1013}{2520} & \frac{41}{45} & \frac{17}{36} & \frac{1}{21} & \frac{1}{2520} & 0 & 0 & 0 & 0 \\
\frac{61}{1260} & \frac{17}{36} & \frac{302}{315} & \frac{397}{840} & \frac{1}{21} & \frac{1}{2520} & 0 & 0 & 0 \\
\frac{1}{2520} & \frac{1}{21} & \frac{397}{840} & \frac{302}{315} & \frac{397}{840} & \frac{1}{21} & \frac{1}{2520} & 0 & 0 \\
0 & \ddots & \ddots & \ddots & \ddots & \ddots & \ddots & \ddots & 0 \\
0 & 0 & \frac{1}{2520} & \frac{1}{21} & \frac{397}{840} & \frac{302}{315} & \frac{397}{840} & \frac{1}{21} & \frac{1}{2520} \\
0 & 0 & 0 & \frac{1}{2520} & \frac{1}{21} & \frac{397}{840} & \frac{302}{315} & \frac{17}{36} & \frac{61}{1260} \\
0 & 0 & 0 & 0 & \frac{1}{2520} & \frac{1}{21} & \frac{17}{36} & \frac{41}{45} & \frac{1013}{2520} \\
0 & 0 & 0 & 0 & 0 & \frac{1}{2520} & \frac{61}{1260} & \frac{1013}{2520} & \frac{451}{630}
\end{bmatrix},$$

$$C^{\mathsf{T}} = [c_0, c_2, c_4, \ldots, c_{N-4}, c_{N-2}, c_N],$$

and

$$F = \begin{bmatrix}
\left(\frac{443}{960}C_{(0)} + \frac{9239}{20160}C_{(1)} + \frac{1019}{5040}C_{(2)} + \frac{1679}{40320}C_{(3)} + \frac{31}{10080}C_{(4)} + \frac{1}{40320}C_{(5)}\right) \\
\left(\frac{19}{160}C_{(0)} + \frac{3361}{8064}C_{(1)} + \frac{1207}{2016}C_{(2)} + \frac{18481}{40320}C_{(3)} + \frac{247}{1260}C_{(4)} + \frac{559}{13440}C_{(5)} + \frac{31}{10080}C_{(6)} + \frac{1}{40320}C_{(7)}\right) \\
\left(\frac{1}{320}C_{(0)} + \frac{419}{10080}C_{(1)} + \frac{247}{1260}C_{(2)} + \frac{9241}{20160}C_{(3)} + \frac{337}{560}C_{(4)} + \frac{9241}{20160}C_{(5)} + \frac{247}{1260}C_{(6)} + \frac{559}{13440}C_{(7)} + \frac{31}{10080}C_{(8)} + \frac{1}{40320}C_{(9)}\right) \\
\left(\frac{1}{40320}C_{(1)} + \frac{31}{10080}C_{(2)} + \frac{559}{13440}C_{(3)} + \frac{247}{1260}C_{(4)} + \frac{9241}{20160}C_{(5)} + \frac{337}{560}C_{(6)} + \frac{9241}{20160}C_{(7)} + \frac{247}{1260}C_{(8)} + \frac{559}{13440}C_{(9)} + \frac{31}{10080}C_{(10)} + \frac{1}{40320}C_{(11)}\right) \\
\left(\frac{1}{40320}C_{(N-11)} + \frac{31}{10080}C_{(N-10)} + \frac{559}{13440}C_{(N-9)} + \frac{247}{1260}C_{(N-8)} + \frac{9241}{20160}C_{(N-7)} + \frac{337}{560}C_{(N-6)} + \frac{9241}{20160}C_{(N-5)} + \frac{247}{1260}C_{(N-4)} + \frac{559}{13440}C_{(N-3)} + \frac{31}{10080}C_{(N-2)} + \frac{1}{40320}C_{(N-1)}\right) \\
\left(\frac{1}{40320}C_{(N-9)} + \frac{31}{10080}C_{(N-8)} + \frac{559}{13440}C_{(N-7)} + \frac{247}{1260}C_{(N-6)} + \frac{9241}{20160}C_{(N-5)} + \frac{337}{560}C_{(N-4)} + \frac{9241}{20160}C_{(N-3)} + \frac{247}{1260}C_{(N-2)} + \frac{419}{10080}C_{(N-1)} + \frac{1}{320}C_{(N)}\right) \\
\left(\frac{1}{40320}C_{(N-7)} + \frac{31}{10080}C_{(N-6)} + \frac{559}{13440}C_{(N-5)} + \frac{247}{1260}C_{(N-4)} + \frac{18481}{40320}C_{(N-3)} + \frac{1207}{2016}C_{(N-2)} + \frac{3361}{8064}C_{(N-1)} + \frac{19}{160}C_{(N)}\right) \\
\left(\frac{1}{40320}C_{(N-5)} + \frac{31}{10080}C_{(N-4)} + \frac{1679}{40320}C_{(N-3)} + \frac{1019}{5040}C_{(N-2)} + \frac{9239}{20160}C_{(N-1)} + \frac{443}{960}C_{(N)}\right)
\end{bmatrix}$$

A posteriori there can be calculated

$$c_{-2} = 2c_0 - c_2, \qquad c_{N+2} = 2c_N - c_{N-2}. \tag{20}$$

The decomposition is continued by solving the linear system

$$(P_h - P_{2h})f(x_{2i-1}) = \sum_{j=1}^{N/2} d_j \Psi_j^J(x_{2i-1}), \tag{21}$$

where $P_{2h}f$ is now the best approximant, and $i = 1, 2, \ldots, M = N/2$. Coarse grid values are readily calculated using the convolution

$$(P_{2h})\, f(x_k) = \frac{1}{48}\left[c_{k-3} + 23\,(c_{k-1} + c_{k+1}) + c_{k+3}\right]. \tag{22}$$

The system matrix P for equation (21) has bandwidth 7, and its elements are $P_{ij} = \Psi_j^J(x_{2i-1})$. Table 2 contains the nonzero elements of columns 1–4. Columns $j = 5, 6, \ldots, M-4$ have zero elements except for $P_{j-k,j} = P_{4-k,4}$, with $-3 \le k \le 3$. The elements of the last three columns satisfy $P_{M-k,M-j} = P_{k+1,j+1}$, $j = 0, \ldots, 3$; $k = 0, \ldots, M-1$.

Table 2.

System Matrix P				
i	$P_{i,1}$	$P_{i,2}$	$P_{i,3}$	$P_{i,4}$
1	$\frac{613572069}{249777920}$	$\frac{-19114505}{1348800768}$	$\frac{6604091}{1348800768}$	$\frac{1}{241920}$
2	$\frac{-29086299833}{47208026880}$	$\frac{-1475969333}{5901003360}$	$\frac{-111788779}{2360401344}$	$\frac{197}{40320}$
3	$\frac{1039839173}{47208026880}$	$\frac{-11642629}{245875140}$	$\frac{-1302921391}{5245336320}$	$\frac{-1273}{26880}$
4	$\frac{1}{241920}$	$\frac{197}{40320}$	$\frac{-1273}{26880}$	$\frac{-15023}{60480}$
5	0	$\frac{1}{241920}$	$\frac{197}{40320}$	$\frac{-1273}{26880}$
6	0	0	$\frac{1}{241920}$	$\frac{197}{40320}$
7	0	0	0	$\frac{1}{241920}$

5. RECONSTRUCTION BY DYNAMIC MOVING AVERAGES

The reconstruction problem, which is the inverse of decomposition, requires an algorithm which combines the coefficients c_k^{J-1}, d_k^{J-1} obtained from solving equations (19) and (21), to regain the coefficients c_l^J, $l = -1, 0, 1, \ldots, N+1$ of equation (9). Viewing equation (13), there will be individual contributions

$$C_l^J = a_l^J + b_l^J \tag{23}$$

from the separate basis function expansions for $P_{2h}f$ and W_hf. It is an easy exercise to show that $P_{2h}f$ contributes as follows:

$$a_{2k}^J = \sum_{j=-1}^{1} p_{-2j} c_{k+j}^{J-1}, \qquad k = 0, 1, \ldots, \frac{N}{2}, \tag{24}$$

$$a_{2k+1}^J = \sum_{j=0}^{1} p_{1-2j} c_{k+j}^{J-1}, \qquad k = 0, 1, \ldots, \frac{N}{2} - 1. \tag{25}$$

Here $c_l^{J-1} = c_{2l}$, where c_{2l} comes from solving equation (14), and the P_l are defined by equations (4) and (5).

Likewise, the contributions from $W_h(x)$ are given by

$$b_{2k}^J = \sum_{j=-2}^{3} q_{-(2j-1)}^{k+j} d_{k+j}^{J-1} \tag{26}$$

and

$$b_{2k+1}^{J} = \sum_{j=-3}^{3} q_{-2j}^{k+j+1} d_{k+j+1}^{J-1}. \tag{27}$$

Here, $d_l^{J-1} = d_l$ results from solving equation (21), and q_k^l is a coefficient from the two-scale relation for wavelet ψ_l (see Table 1), where, for an inner wavelet, the zero index value for k refers to the center of symmetry. For a boundary wavelet the center of indexing is, again, the 6^{th} nonzero coefficient, but moving from the interior towards the boundary with which it is associated. (It is noted that the so-called third boundary wavelet has six nonzero coefficients to one side of the center of indexing, and five to the other side, whereas an inner wavelet has five coefficients to either side.)

Interpretation as a Moving Average

By the well-known method of up-sampling (insertion of zeros to get the vector $c_{-1}, 0, c_0, 0, c_1, 0, c_2, \ldots, 0, c_{N/2}, 0, c_{N/2+1}, 0$) the two formulas of equations (24),(25) can be combined into the moving average scheme

$$a_l^J = \sum_{j=-2}^{2} p_{-j} c_{l+j}^{J-1}. \tag{28}$$

Likewise, by upsampling the d_k^{J-1}, the two equations (26),(27) can be represented by the single *dynamic moving average*

$$b_l^J = \sum_{j=-6}^{6} q_{-j}^{l+j} d_{l+j}^{J-1}. \tag{29}$$

Both equations (28),(29) require index values $l = 0, 1, 2, \ldots, N$ with *a posteriori* calculation (the natural spline condition) of

$$c_{-1}^J = 2c_0^J - c_1^J \qquad c_{N+1}^J = 2c_N^J - c_{N-1}^J. \tag{30}$$

In these equations, $d_i = 0$ if $i < 1$ or $i > N - 1$. Except for third boundary wavelet(s), $q_{\pm 6}^l = 0$.

6. PROVING THE ALGORITHM

As significant computer aided algebra has been accomplished in deriving the present decomposition algorithm, the first experiment is aimed at verification of accuracy. For cubic splines having two continuous derivatives, one should be able to detect discontinuities in a function and its first or second derivatives by performing a wavelet decomposition. Further, use of boundary wavelets and the frontal decomposition technique should eliminate the boundary errors which arise when countable infinite weight sequences are truncated, in adapting wavelet methods for $L_2(R)$ to the interval.

For this purpose, we use the test functions $f_1(x)$ and $f_2(x)$

$$f_1(x) = \begin{cases} -\dfrac{1}{39}(2x-1)\left(4(2x-1)^2 + 32x - 3\right), & \text{if } 0 \le x \le \dfrac{1}{2}, \\ -\dfrac{1}{6}(2x-1)(2x-2)(2x-3), & \text{if } \dfrac{1}{2} < x \le 1, \end{cases}$$

$$f_2(x) = \begin{cases} \dfrac{1}{1+(2x-1)^2}, & \text{if } 0 \le x \le \dfrac{1}{2}, \\ \dfrac{2}{\sqrt{e}} e^x - 2x, & \text{if } \dfrac{1}{2} < x \le 1, \end{cases}$$

interpolated on 128 points, with grid spacing 2^{-7}. Figure 5 shows the first function and its wavelet part (a plot of the wavelet coefficients); Figure 6 shows corresponding results for the

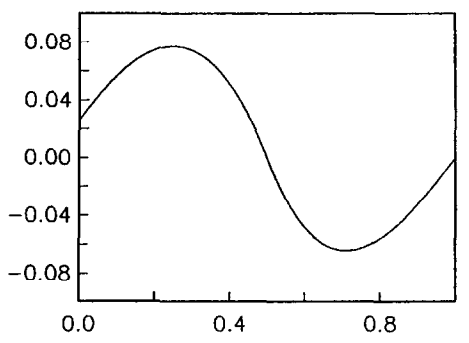

(a) First test function.

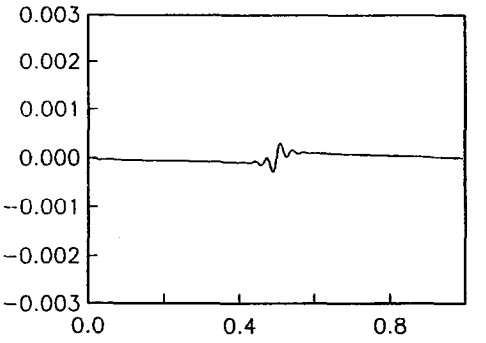

(b) Wavelet coefficients ($j = 7$).

Figure 5.

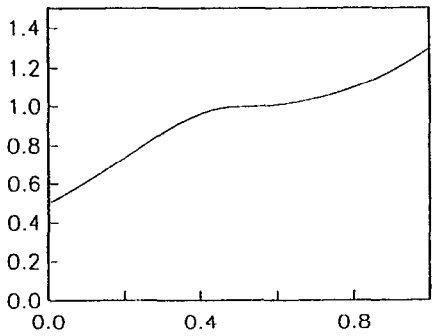

(a) Second test function.

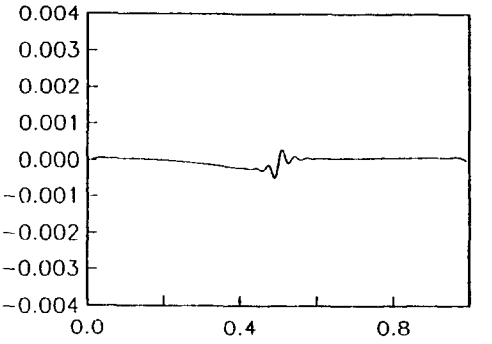

(b) Wavelet coefficients ($j = 7$).

Figure 6.

second test function. Although the derivative discontinuity at the center of the interval is not visible (Figure 5a) in plotting a test function, its detection by observance of wavelet coefficients (Figure 5b) is well localized and accurately space centered, even though the wavelet coefficients are of small magnitude. Further, the usual boundary layer of error at endpoints, which is associated with weight sequence truncation [3], is seen to have been avoided. But, this is the point of using boundary wavelets; hence, the major criteria for success of the present method clearly has been achieved.

7. SOFT THRESHOLD DENOISING WITH WAVELET COEFFICIENTS

A question frequently posed by the user community regards knowing the circumstances under which one type of wavelet may or may not be superior to another. The question is explored here in the context of an application of wavelets to data smoothing called thresholding in the wavelet transform domain. The cubic wavelet structure developed in Section 3 (see Table 1) is now applied to data smoothing in the thresholding context, to determine whether semiorthogonal wavelets can compete with the successes of orthogonal wavelets in this area.

Donoho and Johnstone [10–13] have proposed a very simple procedure for recovering functions from noisy data, which attempts to reject noise by thresholding in the wavelet transform domain. When the wavelet transform utilizes an orthogonal wavelet, the data smoothing which results by thresholding is claimed to be very good [11].

The objective in this section is to report some numerical experiments where the thresholding technique is attempted, for the case in which the wavelet transform utilizes the semiorthogonal cubic B-spline wavelet and the interval MRA algorithm developed in Sections 3 and 4. The best that can be said is that some degree of data smoothing is obtained; however, the level of variance reduction is insufficient for acclaim to be credited to the method. Evidently the property of an

orthogonal transform of the data, strongly utilized in theoretical studies of Donoho's method, is crucial to significant variance reduction.

Suppose it is desired to recover an unknown function $f(t_i)$ defined on $[a, b]$ from noisy data

$$d_i = f(t_i) + \sigma Z_i, \qquad i = 0, 1, 2, \ldots, n-1 \tag{31}$$

where $t_i = \dfrac{i}{n}$

$Z_i \sim N(0,1)$ Gaussian white noise

σ noise level.

One interpretation of the term "denoising" is that one's goal is to optimize the mean-squared error

$$E\|f_n^*(t_i) - f(t_i)\|_{l_n^2}^2 = \sum_{i=0}^{n-1} E\left\{f_n^*\left(\frac{i}{n}\right) - f\left(\frac{i}{n}\right)\right\}^2.$$

The denoising process, which is not necessarily optimal, follows. First, the interval-adapted cubic B-spline wavelet and natural spline MRA of Sections 3 and 4 are employed to "wavelet transform" the data by decomposition over several levels of increasing coarseness. Next, the resulting wavelet coefficients are translated towards zero, by applying the soft threshold nonlinearity

$$\eta_t(y) = \operatorname{sgn}(y)(|y| - t)_+$$

where

$$\operatorname{sgn}(y) = \begin{cases} 1, & \text{if } y > 0, \\ 0, & \text{if } y = 0, \\ -1, & \text{if } y < 0, \end{cases} \tag{32}$$

$$(|y| - t)_+ = \begin{cases} |y| - t, & \text{if } |y| > t, \\ 0, & \text{elsewhere}, \end{cases} \tag{33}$$

coordinatewise to the wavelets coefficients, with specially chosen values for the threshold t. Upon reversing the pyramid filtering process (by reconstruction), the smoothed values $f_n^*(i/n)$, $i = 0, 1, 2, \ldots, n-1$, are recovered.

Table 3. Smoothing by projection only.

Level	R.M.S. Deviation
$j = 8$	0.30634297538607
$j = 7$	0.37763354502562
$j = 6$	0.29557825406323
$j = 5$	0.30936344208145
$j = 4$	0.16003431015278
$j = 3$	0.13060963413918

Table 4. Reconstruction with threshold (t).

Multilevel reconstruction over 5 Levels	
Threshold	R.M.S. Deviation
$t = 0.5$	0.44165132955322
$t = 1$	0.33079362895004
$t = 1.5$	0.25484707840785
$t = 2$	0.20541018868544
$t = 3$	0.17873406305794

A Data Smoothing Experiment

The outcome of some numerical experiments which implement the denoising technique are now reported. A graduated sequence of t-values are employed for the natural B-spline wavelets as seen in Table 4. The corrupting signal is white (Gaussian) noise from a random number generator,

which is added to a sinusoidal input sampled over the interval $[0, 2\pi]$. Numerical results are shown below. Table 3 shows the smoothing accomplished by the natural B-spline wavelets simply projecting from the fine grid to a coarser grid level, with no thresholding. Table 4 shows the effects of thresholding several coarse levels after reconstructing back to the fine level. There is a progression in quality of the resulting data smoothing as the threshold varies, as may be seen from Table 4. Indeed, as the threshold approaches $t = 3.0$, it is seen in Table 4 that the standard deviation converges to 0.178734.

Figures 7–9 depict projected data, wavelet coefficients, and reconstructed data over several levels. From the appearance of the wavelet transform coefficients, one might suspect that the random noise generator is producing correlated noise in the vicinity of $x = 5.0$.

It is seen that Donoho and Johnstone's soft thresholding method in conjunction with the semiorthogonal wavelet lead to numerical experiments whose resulting smoothing recovery from an unknown noisy data is, at best, about the 15% level in variance reduction. Indeed, as a result of simply projecting to the fourth level ($j = 4$) of coarseness, we get better smoothing results than are obtainable by thresholding, as may be seen from Table 3.

Smoothing a Corrupted Sine Wave

$$d_i = f(t_i) + \sigma Z_i, \qquad i = 0, 1, 2, \ldots, n-1$$

where $t_i = \dfrac{i}{n}$

$Z_i \sim N(0,1)$ Gaussian white noise

$\sigma = 1.$

$f(t_i) = \sin(t_i)$

Wavelet transform $\overline{d}$ = A soft thresholded wavelet coefficient

$$\text{Variance} \sum_i \frac{\left(\overline{d_i} - f(t_i)\right)^2}{n}$$

$$\text{R.M.S. deviation } \sqrt{\text{Variance}}$$

$$\text{R.E.} \frac{\left\| f(x) - \widehat{f(x)} \right\|}{\|f(x)\|}$$

8. DATA COMPRESSION BY QUANTILE THRESHOLDING

In the last few years the advent of multimedia computing has initiated a revolution in research concerning image compression. Here, storage and manipulation of image data in raw form can be very expensive. For example, a standard 35 mm photograph digitized at $12\,\mu$m per pixel requires about 18 MBytes of storage, and one second of NTSC-quality color video requires about 23 MBytes of storage [14]. High definition television (HDTV) is another area where sheer volume of data which must be transported and stored (in real time) boggles the imagination.

It is clear that in order to take advantage of what is becoming cutting edge technology in these areas, some form of data compression is necessary. Indeed, the introduction of the wavelet concept has spurred a revolution in the field of data compression.

In this section, we investigate the quality of data compression that can be obtained from lossy compression schemes which employ the interval wavelets derived in Section 3 (see Table 1). Basically, there are two different kinds of schemes for compression: lossless and lossy. In the case of lossless compression, one is interested in reconstructing the data exactly, without loss of

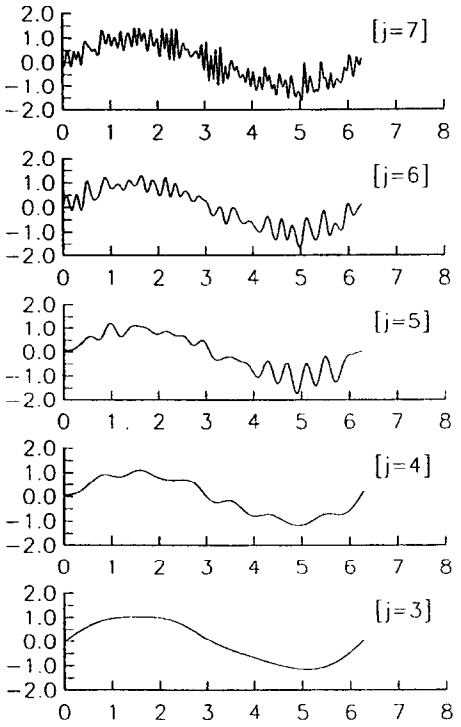

Figure 7. Multilevel decomposition with noisy signal.

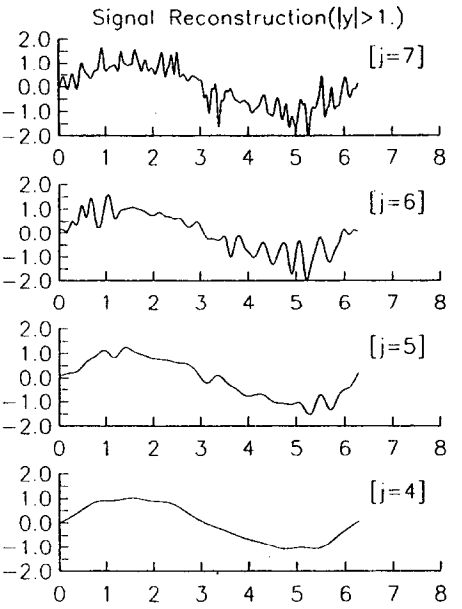

Figure 8. Signal reconstruction ($t = 1$).

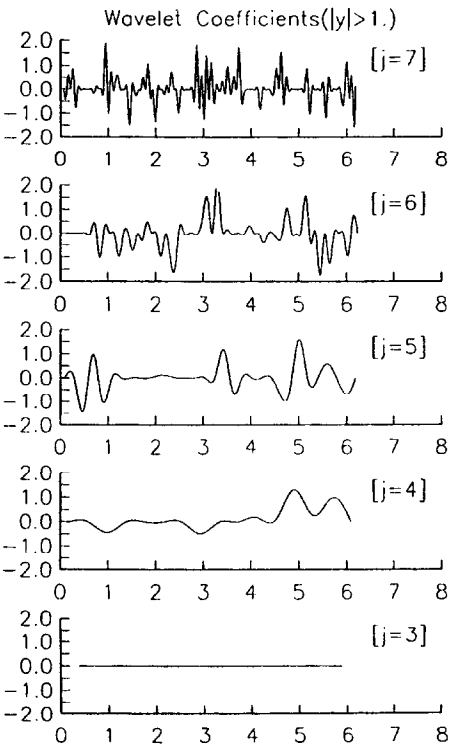

Figure 9. Wavelet coefficients ($t = 1$).

information, such as with Huffman Coding [15]. Lossy compression is considered here, where error is permitted, as long as image quality after reconstruction is acceptable. In general, much higher compression ratios can be obtained with lossy schemes than those characterized by lossless

compression.

Loss or distortion introduced in reconstruction shall be defined as the R.M.S. or l^2 norm of the difference between $f(x)$ and its approximation $\widehat{f(x)}$. For simplicity of comparison, this shall be normalized to the relative difference $\|f(x) - \widehat{f(x)}\|/\|f(x)\|$.

Signals which are of interest in data compression application are usually characterized by a time-varying frequency. One such signal is $y = \sin(t^2)$, which is to be used for numerical experiments. Interest is focused on a data window of length $N = 2^n$, where $n = 10$. Using the techniques of Section 4 involving multiresolution analysis on the interval, this data will be decomposed to a level of coarseness $n = 3$, with quantile thresholding of the wavelet coefficients.

Table 5. Data cutoff by compression on 1024 points.

Level	Cutoff($\epsilon = 0.001$)	Cutoff($\epsilon = 0.01$)	Cutoff($\epsilon = 0.1$)
$j = 9$	308	414	512
$j = 8$	146	174	234
$j = 7$	66	76	96
$j = 6$	31	34	37
$j = 5$	16	16	19
$j = 4$	9	9	15
$j = 3$	2	2	4
Remaining Data	438	291	99
R.M.S.	4.11×10^{-3}	4.07×10^{-3}	4.45×10^{-3}
R.E.	5.91×10^{-3}	5.86×10^{-3}	6.41×10^{-3}

Table 6. Data cutoff by compression on 1024 points.

Level	Cutoff($\epsilon = 1$)	Cutoff($\epsilon = 2$)	Cutoff($\epsilon = 5$)
$j = 9$	512	512	512
$j = 8$	256	256	256
$j = 7$	119	127	128
$j = 6$	48	49	53
$j = 5$	24	27	27
$j = 4$	15	15	16
$j = 3$	6	7	8
Remaining Data	36	23	16
R.M.S.	4.45×10^{-3}	4.45×10^{-3}	4.45×10^{-3}
R.E.	6.41×10^{-3}	6.41×10^{-3}	6.41×10^{-3}

Since distortions up to 5% are considered acceptable in some speech processing applications, an optimal compression method for a deterministic signal is one that yields no more than 5% distortion while maximizing the compression ratio. Though the quality of the restored signal may be criticized in some cases, the data compression results from wavelet signal analysis shown in Tables 5 and 6 are, perhaps, amazing. For best case compression, to approximately reconstruct the original 1024 word signal requires only 24 data nonzero values to be stored. This is a compression ratio of about 40 to 1.

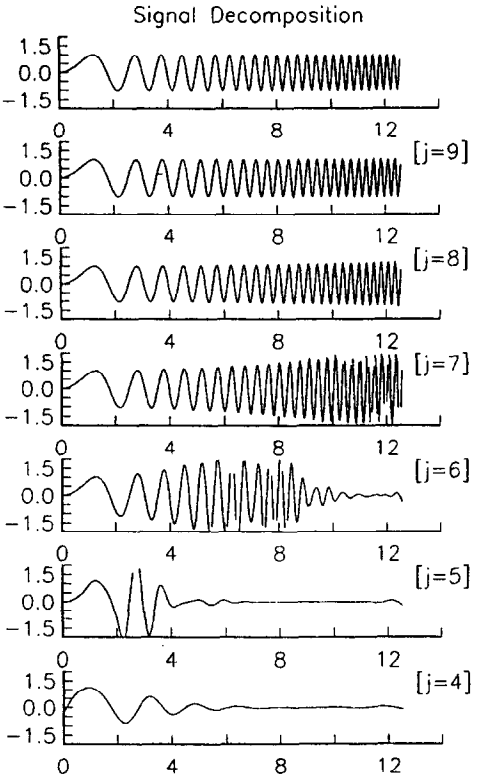

Figure 10. Multilevel decomposition $y = \sin(x^2)$.

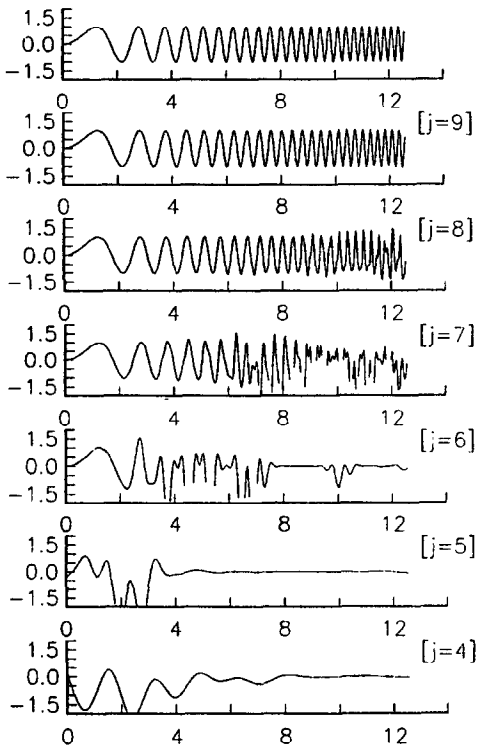

Figure 11. Signal reconstruction ($\epsilon = 0.1$).

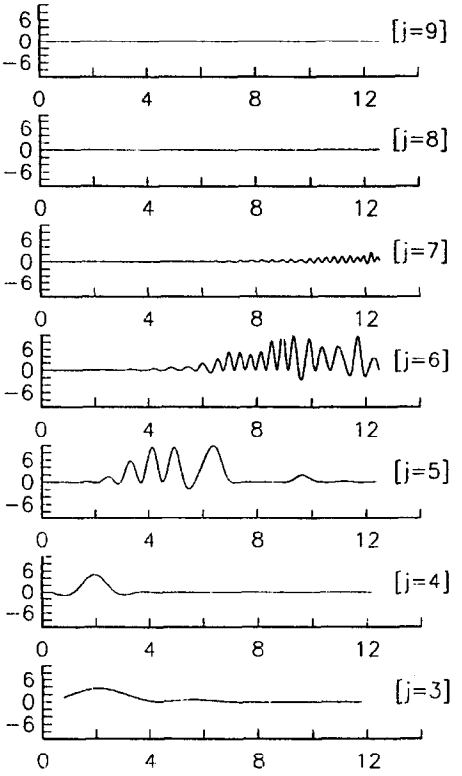

Figure 12. Wavelet coefficients ($\epsilon = 0.1$).

The rule for thresholding is given as

$$d_j^{\text{quant}} = \begin{cases} 0, & \text{if } d_j < \epsilon, \\ d_j, & \text{if } d_j \geq \epsilon. \end{cases}$$

Results for reconstruction when the value $\epsilon = 0.01$ is used are shown in Figures 11 and 12. When reconstructing to the original signal, R.E. and R.M.S. errors converge to 6.4×10^{-3} and 4.5×10^{-3}, as shown in Tables 5 and 6.

9. CONCLUSION

A Maple derivation of new boundary wavelets which accompany the cubic inner spline wavelet of Chui-Quak [1] has been presented, together with a frontal technique for decomposition over a finite interval of functions contained in the MRA generated by a piecewise cubic B-spline local basis. The technique avoids the use of pyramid schemes and the necessity of truncating weight sequences of infinite length, which procedure would appear to lower the accuracy of the B-wavelet. Numerical experiments indicate excellent results for the frontal method of decomposition, as regards both accuracy and efficiency of the algorithm. The problem of boundary error is well disposed of by the present scheme, where boundary scaling functions with multiple nodes [1,6] at interval endpoints have been avoided by use of more natural scaling functions. Moreover, this approach apparently gives results which are equivalent to those of [6], with improved algorithm efficiency. Data smoothing by means of thresholding in the wavelet transform domain is not as successful for semiorthogonal wavelets as it has been advertised for orthogonal wavelets. On the other hand, very good results are achieved for a data compression scheme which employs these interval wavelets. A compression ratio of 40 to 1 is experienced.

REFERENCES

1. C.K. Chui and E. Quak, Wavelets on a bounded interval, In *Numerical Methods of Approximation Theory*, Volume 9, (Edited by D. Braess and Schumaker), pp. 53–75, Birkhäuser, Basel, (1992,).
2. Y. Sang and C.H. Cooke, Multi-resolution analysis on the interval with spline wavelets which maintain a uniform two-scale relation, *Journal of Scientific Computing* (to appear).
3. C.K. Chui, *An Introduction to Wavelets*, Academic Press, (1992).
4. I. Daubechies, *Ten Lectures on Wavelets*, CBMS-NSF Regional Conference Series in Applied Mathematics, Volume 61, SIAM, (1992).
5. A. Cohen, I. Daubechies and P. Vial, Wavelets on the interval and fast wavelet transforms, In *Comptes Rendus*, Acad. Sci., Paris, (1992).
6. E. Quak and N. Weyrich, Decomposition and reconstruction algorithms for spline wavelets on a bounded interval, Report 294, Center for Approximation Theory, Texas A&M University, College Station, TX, (April 1993).
7. Y. Meyer, Ondelettes sur l'intervalle, *Rev. Mat. Ibero-americana* **7**, 115–143 (1991).
8. S. Mallat, A theory for multiresolution signal decomposition: The wavelet representation, *IEEE Trans. Pattern Analys. and Machine Intell.* **11**, 674–693 (1989).
9. L.L. Schumaker, *Spline Functions: Basic Theory*, John Wiley, New York, (1981).
10. D.L. Donoho, De-noising by soft thresholding, In *Proceedings of the Symposium on Wavelet Theory*, Vanderbilt University, April 3–4, 1992.
11. D.L. Donoho, Unconditional Bases are optimal bases for data compression, Technical Report, Department of Statistics, Stanford University, (1992).
12. D.L. Donoho, Wavelet shrinkage and W. V. D.: A 10-minute tour, Technical Report, Stanford University, (1993).
13. D.L. Donoho and I.M. Johnstone, Minimax estimation by wavelet shrinkage, Technical Report, Department of Statistics, Stanford University, (1992).
14. M.L. Hilton, B.D. Jawerth and A. Sengupta, Compressing still and moving images with wavelets, *Multimedia Systems* **2** (3) (1994).
15. M.V. Wickerhauser, Acoustic signal compression with wavelet packets, In *Wavelets: A Tutorial in Theory and Applications*, Vol. 2, (Edited by C.K. Chui), pp. 679–700, Academic Press, San Diego, (1992).
16. R.L. Fante, *An Introduction to Signal Analysis and Estimation*, John Wiley & Sons, New York, (1988).